Science of Sintering, **52** (2020) 387-403

https://doi.org/10.2298/SOS2004387H

UDK: 666.3.019; 622.785; 546.65

High Macroscopic Neutron Capture Cross Section Ceramics Based on Bauxite and Gd_2O_3

María F. Hernández[1,2], María S. Herrera[3], Ricardo Anaya[3], Juan Manuel Martinez[1,2], Mariano Cipollone[3], María S. Conconi[1,2], Nicolás M. Rendtorff[1,2*)]

[1]Centro de Tecnología de Recursos Minerales y Cerámica (CETMIC): (CIC-CONICET-CCT La Plata), Camino Centenario y 506 s/n, C.C.49 (B1897ZCA) M.B. Gonnet, Argentina.

[2]Dpto. De Química, Facultad de Ciencias Exactas, Universidad Nacional de La Plata, UNLP, 47 y 115 s/n, La Plata, Argentina.

[3]YPF Tecnología S.A., CONICET, Av. del Petróleo s/n e 129 y 143, (1923) Berisso, Buenos Aires, Argentina.

Abstract:

The effect of the addition of Gadolinium oxide (Gd_2O_3) up to 10 wt.% in bauxite was studied and its thermal behavior compared with pure bauxite. The incorporation of Gd_2O_3 is of technological interest for the design of smart traceable ceramic proppants used for unconventional gas and oil well stimulation. These high macroscopic neutron capture cross section proppants are used to obtain relevant information, such as the location and height of the created hydraulic fractures, through a neutron based detection technology. The study comprised a set of thermal and sintering behavior analyses up to 1500 °C of mixtures up to 10 wt.% addition of Gd_2O_3. The developed texture and microstructure was also assessed. A simple mechanical characterization was performed as well. Fully-dense pore-free microstructures were developed, with alumina and mullite as the main crystalline phases. Gadolinium secondary and ternary alumino-silicate phases were also observed after thermal treatment. These present a needle morphology that might result in reinforcement mechanisms. No important glassy phase was detected; although sintering was enhanced, the Gd_2O_3 oxide main role was found to be as a sintering aid rather than a strict flux agent. The mechanical behavior remained fragile with the rare oxide addition. In fact, the mechanical resistance increased up to 20 wt.% for the 10 wt.% added sample. The oxide addition together with the bauxite dehydroxilation mass loss resulted in materials with up to 1.5 x 105 (c.u.) macroscopic neutron capture cross section materials. The obtained results permit to define design strategies of high macroscopic neutron capture ceramic materials for wellbore and developed fractures description.

Keywords*: Bauxite; Rare earth; Gadolinium oxide; Smart ceramic proppants; Thermal neutron capture cross section.*

1. Introduction

Ceramic proppants are frequently used in hydraulic fracturing of unconventional oil and gas reservoirs. Each hydraulic stimulation uses of about 230 tons per year of proppants.

*) **Corresponding author:** rendtorff@cetmic.unlp.edu.ar

The proppant specifications are ruled by the American Petroleum Institute (API) and their main requirements are: grain distribution size, sphericity, roundness, crush resistance, acid solubility, turbidity and hydraulic conductivity. Sintered proppants are developed to achieve fluid and gas conductivities under rigorous conditions of deep environments. They should maintain their integrity under high temperature, salinity and acidity during usage [1]. Ceramic proppants have widely demonstrated their suitability to fulfill these requirements with a good cost-availability-performance relation. Ceramic proppants belong to the Al_2O_3-SiO_2 system and are manufactured from bauxite and/or kaolin clays (US Patent 8,234,072 B2); [2-5].

After the well stimulation process, it is highly desirable to know the fracture geometry and proppants distribution in it. Recently, methods to identify proppants in induced formation fractures have been proposed (US Patent 8,234,072 B2, US 8,648,309) and applied [6-9][10-15]. These methods require the incorporation of a suitable high thermal neutron capture element, such as gadolinium or samarium, into the proppant grain during the ceramic manufacturing process. The incorporation is accomplished by adding oxides or other derived compounds of these elements to the starting raw powder (US Patent 8,234,072 B2). These are known as traceable smart proppants, which have a high avidity for absorbing slow or "thermal" neutrons (energy < 0.5 eV).

Physical properties of the tagged proppant (e.g., crash strength and conductivity) are unaffected by the addition of Gd_2O_3 at a low concentration (0.025 % to 1 % by weight of the proppant) (US Patent 8,234,072 B2). The rare earth incorporation increases the thermal neutron capture cross section (σ) of the constituent proppant material and makes it detectable by the depression of the thermal neutron flux, or due to the emitted gamma rays (prompt gamma rays) [16].

The addition of elements such as gadolinium (49,700 b) and samarium (5,922 b) increases the macroscopic thermal neutron capture cross section of the proppant and makes it detectable after placement in the fracture. This is mainly achieved by measuring the suppression of the thermal neutron flux recorded in the post-frac log, or by computing the gadolinium yield through gamma spectroscopy. After-fracture signals are often compared to the corresponding before-fracture signals, showing the presence (or absence) of the traceable material. Up to date there is only one traceable proppant (ceramic) available in the market which uses gadolinium oxide[17,18]. The technology has been successfully employed over 200 vertical wells in field operations in the last decade [7-9, 16-20].

It is common in petrophysics to use the macroscopic capture cross section (Σ) as a bulk property for neutron interactions with materials. This parameter is defined as the product of σ and the number of atoms per cubic centimeter *N* [21]:

$$\Sigma_i = N\sigma_i = \frac{N_{av}\,\rho}{A}\sigma_i \qquad (1)$$

Where, N_{av} is Avogadro's number, ρ is the density (in g.cm^{-3}), and *A* is the atomic weight of the isotope. Note that Σ has dimensions of cm^{-1}, however, the so-called capture units (c.u.) are preferably used in petrophysics, multiplying 1000 times ∑. This can be estimated from the composition density information of the materials [16, 18], and (qualitatively) illustrates the detectability of the proppants. Although commercial ceramic proppants, CarboNRT®, use up to 0.4 wt.% of gadolinium oxide addition in their composition, higher concentrated proppants (ultra detectable) could be easily blended with non-tagged proppants in order to achieve adequate detectable mixtures. This approach in the use of traceable smart proppants requires a better understanding of the ceramic behavior of gadolinium oxide in higher proportions, in order to obtain ceramic design strategies.

In a previous article we performed a systematic thermal behavior study of kaolinitic clays mixtures with gadolinium oxide and samarium oxide, due to the same technological

interest of these thermochemical processes [10, 11]. A systematic formulation-sintering-properties correlation was carried out. The thermo-chemical complex processes were not considerably affected by the presence of the Gd_2O_3. The resultant materials were like the non-tagged material, and have gathered all the properties for proppants fabrication. Because of these, the thermal behaviors of bauxite mixtures with gadolinium oxide are of technological interest.

1.1 Objectives

In this work we describe the effect of gadolinium oxide addition in the thermal behavior of bauxite and evaluate the changes in the technological properties of the resulting ceramics. This will enlighten the processing strategy of gadolinium based ceramic proppants and allow inferring the processing cost of the study functionalization.

2. Materials and Experimental Procedures

2.1 Materials

An industrial grade bauxite was employed as the model bauxite [2]. The main properties of the employed Bauxite are shown in Table I. Chemical composition was performed by X-Ray Fluorescence Spectrometry, using a Shimadzu Energy Dispersive Spectrometer, model EDX-800HS. The lost on ignition was carried out in a muffle furnace at 1000 °C for one hour. Mineralogical composition was determined by X-Ray Power Diffraction on a Philips 3020 goniometer with Cu-Kα radiation, Ni filter, at 40 kV-35 mA; with 0.04° and 2 seconds steps in the 3-70° range. Patterns were analyzed with the program FullProf (Version 5.80 – 2016), a multipurpose profile-fitting program, which includes Rietveld refinement to perform phase quantification [14, 22]. A pure gadolinium oxide (Gd_2O_3) (Sigma Aldrich: CAS Number 12064-62-9) 99.9 % purity was employed ($D_{50} \approx 2$ μm).

Tab. I Chemical and mineralogical composition of the employed bauxite.

Oxide composition	**Bauxite**
	wt.%
SiO_2	11.53
Al_2O_3	53.35
Fe_2O_3	5.72
K_2O	0.13
TiO_2	0.65
SO_3	0.13
LOI (dry samples)	27.97
Mineralogical	**wt.%**
Gibbsite ($Al(OH)_3$)	72
Kaolinite ($Al_2O_3.2SiO_2.2H_2O$)	23
Boehmite (AlO(OH))	2
Maghemite (Fe_2O_3)	3

2.1 Mixture formulations

Mixtures of bauxite containing 1.0, 5.0 and 10.0 % by weight of Gd_2O_3 were studied and labeled as BGd1, BGd5 and BGd10, respectively. They were compared with the pure

bauxite sample, labeled BGd0. The mixture formulations range criteria was to obtain an equivalent macroscopic capture cross-section in such mixtures as the ones present commercial traceable proppants [16, 23].

2.3 Processing: powder mixing and sintering

The chosen processing route was the same as the precedent clay-rare earth mixture study [10]. Bauxite-oxide mixtures were obtained by wet ball milling; alumina jar and milling media were employed. Dried mixtures were de-agglomerated and sieved (#200) before pressing. The disc shape was chosen because they present more controllable dimension and is possible in this shape to measure properties rather than in proppants. The sphere proppants morphology can be obtained only through specific equipment like pelletizing disks or drums, or high energy mixers [1]. The sphere proppants morphology can be obtained only through specific equipment like pelletizing disks or drums, or high energy mixers [1]. The compaction route used here can be regarded as an adequate route due to particular processing variables [23].

In our case, the compaction grade was 55 % of the theoretical density. However, the sintering behavior of ceramic based materials can be qualitatively extrapolated to different conformation processing routes. It is well known that the amount of mullite governs the mechanical properties of clay based ceramic materials [14, 24], hence the disc samples results might be extrapolated to sphere geometries.

Samples were fired at the same heating rate (10 °C/min) with different maximum temperatures at 1250, 1350 and 1400 °C and 30 minutes soaking in air atmosphere.
The employed geometries and pressure are a starting point for further sintering studies that could be carried out after this additive (Gd_2O_3) formulation study. Samples with no, 1, 5 and 10 wt.% were studied and labeled Gd0, Gd1, Gd5 and Gd10 respectively.

2.4 Bauxite – Gd_2O_3 mixtures characterizations

The effect of heat treatment was evaluated by thermogravimetric and differential thermal analysis (DTA-TG) simultaneously carried out on a Rigaku Evo II equipment in air atmosphere, with a 10 °C/min heating rate in Pt crucibles. The derivative curve of the TG (DTG) was also employed for this purpose. To understand the sintering behavior, thermomechanical analysis on a vertical prismatic (20.0 x 3.5 x 3.5 mm^3) sample was performed; with a 10 °C/min heating rate in air atmosphere (TMA Rigaku Evo plus II, Japan) [25, 26].

Sintering studies of the samples were performed using a hot-stage microscope (HSM). Cylindrical specimens (5 mm high and 3 mm in diameter) were prepared by uniaxial pressing. They were placed vertically on the sample holder of the heating microscope oven (L74 Linseis) and were tested with heating ramp of 10 °C min^{-1} up to 1400 °C. The temperature was recorded with a Pt–Rh type S thermocouple. The images captured with the digital camera in the microscope were configured in such a way as to obtain a record of one shot per degree centigrade [27]. Changes of the height L in the course of their heating compared with initial height (L0) of the samples at the starting temperature were determined analyzing sintering process.

The Apparent density and porosity of the fired samples was obtained by the Archimedes immersion method. These two sintering parameters illustrate the actual sinterization grade of the resulting materials; ceramic proppants sintering must be high in order to achieve high strength; the clay thermal shrinkage may be assumed to be isotropic.

Identification of crystalline phases in the fired materials were carried out by X-ray diffraction (XRD) (Philips 3020 with Cu-Kα radiation, Ni filter, at 40 kV–35 mA; with 0.04°

and 2 s steps in the 3–70° range). Phase identification from XRD patterns was carried out using PDF- 2 database (ICDD PDF-2).

Afterward, the microstructure analysis was performed using a scanning electron microscope (SEM: JEOL, JCM- 6000). Surface was analyzed in ultra-high vacuum conditions and 20.0 kV. An Everhart-Thornley Detector (ETD) was employed in back-scattered electron mode. Energy Dispersive Spectroscopy (EDS) analysis was carried out in mapping mode at 15 kV and 7800 seconds of acquisition time.

Finally, a simple comparative mechanical characterization was carried out, evaluating only the optimized materials by diametral compression. This test, also known as “splitting test” or “Brazilian test”, has been usually employed in mechanical evaluation due to several advantages: simpler piece preparation, simple geometry and quickness of testing, independent data with regard to surface finish and no edge effects [10, 28, 29]. In this case, the 15 mm diameter and 5 mm thick disc-shaped samples were diametrically compressed in a universal mechanical testing machine (INSTRON 5985, USA), at a constant strain rate of 0.1 mm/min, with steel plates. Lubricant paste was applied on the platen surfaces in contact with the disc to reduce friction; white and carbon papers were placed together between each platen and the disc for load distribution (padding material). The initial diameter was used for the calculation, and L was employed for the final maximum load of samples. In this method, the mechanical strength and displacement can be calculated with the following equations:

$$\sigma_d = \frac{2L}{\pi DT} \qquad (2)$$

$$\varepsilon = \frac{\Delta d}{D} \qquad (3)$$

At least 8 samples were evaluated for each material, where L is the final load, D is the initial diameter, T is the thickness of the disc-shaped sample and Δd is the universal testing machine displacement.

3. Results and Discussion

3.1 Thermal behavior of the bauxite-oxide mixtures

3.1.1 TG-DTA

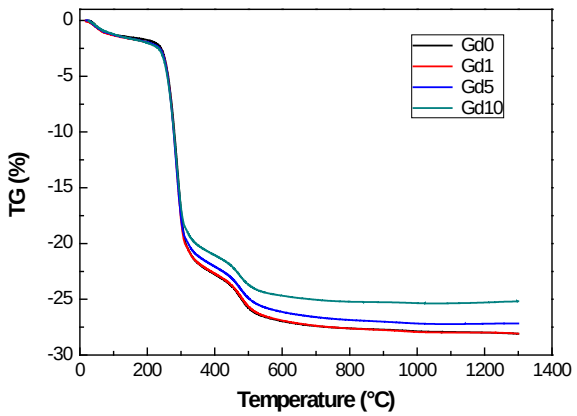

Fig. 1. Thermo gravimetric (TG) curves of the Bauxite - Gd_2O_3 samples.

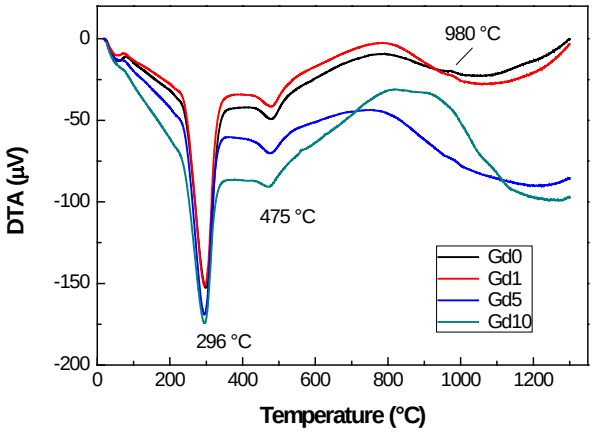

Fig. 2. Differential thermal analysis curves of the (DTA) of the Bauxite - Gd_2O_3 samples.

The TG (Fig. 1) behavior of the bauxite and mixtures are similar. The hydroxide decomposition; (two steps) is clearly observed near 300 and 475 °C down to 22 and 27 % respectively as reported for other bauxites, with kaolinite as secondary mineral [30]. No other mass involved process can be observed in the TG. An expectable dilution effect with the increase in Gd_2O_3 content can be observed, as mass losses decrease with the oxide addition. The two endothermic processes are also observed in the DTA curves, accompanied by a small exothermic peak at 980 °C. This corresponds to the spinel aluminosilicate formation [12, 31, 32]. This is difficult to observe in the Gd10 mixture. No other thermal processes were detected by this method.

3.1.2 HSM - TMA

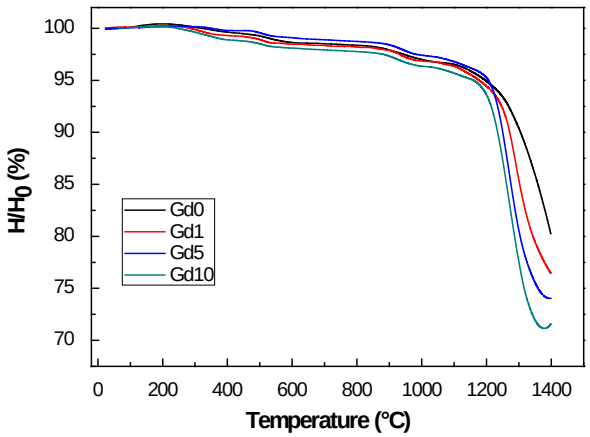

Fig. 3. Sintering curves of the of the Bauxite-Gd_2O_3 samples.

The sintering curves illustrate the shrinkage thermal evolution (Fig. 3). The behavior is similar for the four studied samples: a slight shrinkage is observed up to 1200 °C; with small steps at 300, 500 and 950 °C respectively; each one corresponding to the thermal processes described by the DTA (Fig. 1). The main sintering process starts at 1200 °C, with an abrupt shrinkage. The sintering rate increases with the Gd_2O_3 addition, and the maximum achieved shrinkage is almost 30 % for the Gd10 sample. This value is slightly lower for the pure

bauxite sample. The rare earth addition could be understood as a sintering aid of bauxite since shrinkage rate is rising with Gd content [33, 34]. Above 1350 °C in sample Gd10 a slight enlargement can be observed. This peak might be related to the subsequent chemical processes involved in the reaction sintering (see section 3.2) [25]; evidently developed new phase present a lower density, which results in an enlargement.

The actual processing heating program for industrial development could be optimized after this analysis. Evidently the maturing temperature range is between 1350 and 1450 °C. this corresponds with previous reports [2, 3, 5]. The chosen batch samples temperatures were based on this analysis.

3.2 Developed crystalline and non-crystalline phases

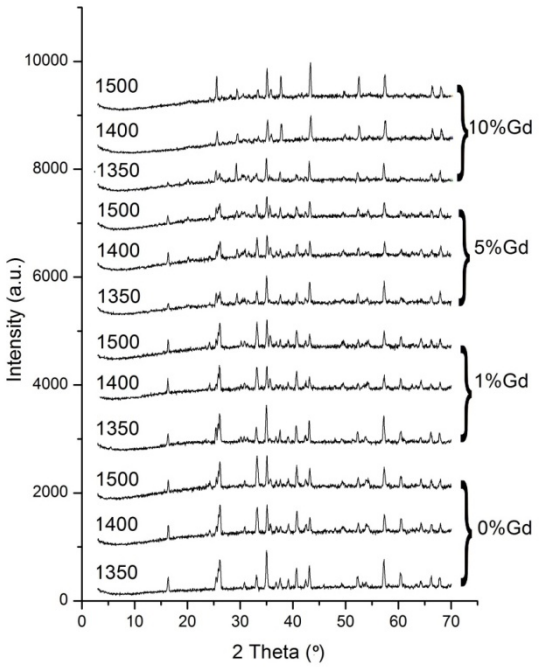

Fig. 4. XRD Patterns of the fired ceramic samples at different final temperature and different rare earth content.

XRD patterns of the studied samples are shown in Fig. 4, the identified crystalline phases are shown in Table II, PDF files are shown as well.

As expected, the sintered bauxite resulted in Coridon (Al_2O_3) and Mullite $3Al_2O_3.2SiO_2$ as principal crystalline phases. These are accompanied by hematite (Fe_2O_3); with no titanium oxide detected; thus these results are considered consistent with the chemical and mineralogical composition of the stating powder (Table I). No other phase was identified, and no important thermal effect was observed in the 1350-1500 °C range. The typical thermochemical processes of the kaolinite alumina mixtures occur below this temperature[12, 35, 36]. The amount of mullite developed (primary and secondary) [37] corresponds to the kaolinite present in the starting raw material [2]. No crystalline silica phases (SiO_2), such as cristobalite or quartz, nor silica based glass were detected. This fact ensures the structural behavior for these kinds of materials.

The incorporation of the rare earth oxide slightly affected the developed crystalline phases. Firstly, the iron phase was partially altered into Maghemite/Magnetite Fe_3O_4 instead of Hematite, and iron silicate was observed (which was not present in the pristine bauxite sample).

Secondly, the mullite content of these samples (Gd5 and Gd10) was decreased or even suppressed; instead, gadolinium silicates or alumino-silicates (see Table II) were identified. In all samples, the principal crystalline phase is the aluminum oxide, ensuring an appropiate mechanical behavior of these materials and the proppant performance [1].

Finally, traces of gadolinium titanate and silicate and iron aluminate were detected in the samples with rare earth oxide, in the high proportion samples Gd5 and Gd10. This is not important, and do not considerably affect the technological properties.

Tab. II Identified crystalline phases in the fired samples.

Phase		**Alumina Al_2O_3**	**Mullite $3Al_2O_3\ 2SiO_2$**	**Hematite Fe_2O_3**	**Maghemite/ Magnetite Fe_2O_3/ Fe_3O_4**	**$Gd_2Si_2O_7$**	**$Gd_{4.67}(SiO_4)_3O$**	**$Al_3Fe_2Gd_3O_{12}$**	**$Gd_2Ti_2O_7$**
		PDF file							
Sample	**Firing temperature (° C)**	**01-080-0786**	**01-089-2645**	**01-073-2234**	**01-089-5892**	**00-026-0662**	**01-072-2070**	**00-015-0205**	**01-073-1698**
Gd0	1350	xxxx	xx	x					
	1400	xxxx	xx	x					
	1500	xxxx	xx	x					
Gd1	1350	xxxx	xx	x	x				x
	1400	xxxx	xx	x	x				x
	1500	xxxx	xx	x	x				x
Gd5	1350	xxxx	xx	x		x	x	x	x
	1400	xxxx	xx	x	x	x	x		x
	1500	xxxx	x	x	x	x	x		x
Gd10	1350	xxxx	x	x	x	x	x		x
	1400	xxxx		x		x	x		x
	1500	xxxx		x		x	x		x

3.3 Sintering parameters and textural properties

After the sintering test, samples were fired at different heating programs with 2-hour dwelling. These conditions are similar to the actual ceramic processing heating programs [3]. Both open porosity and density were evaluated by the immersion test. The open porosity is a

more effective sintering parameter, especially when different crystalline phases are observed. Open porosity decreased from 10.8 to 1.8 % for the parental bauxite (see Fig. 4). In the studied range, open porosity decreased both with maximum temperature and rare earth addition increase. Nearly null open porosity samples were achieved with 1500 °C Gd_2O_3 added samples (Gd1, Gd5 and Gd10).

The apparent densities achieved are also affected by the studied processing variables (see Fig. 5). Apparent density increased with both explored variables increase: temperature and rare earth addition.

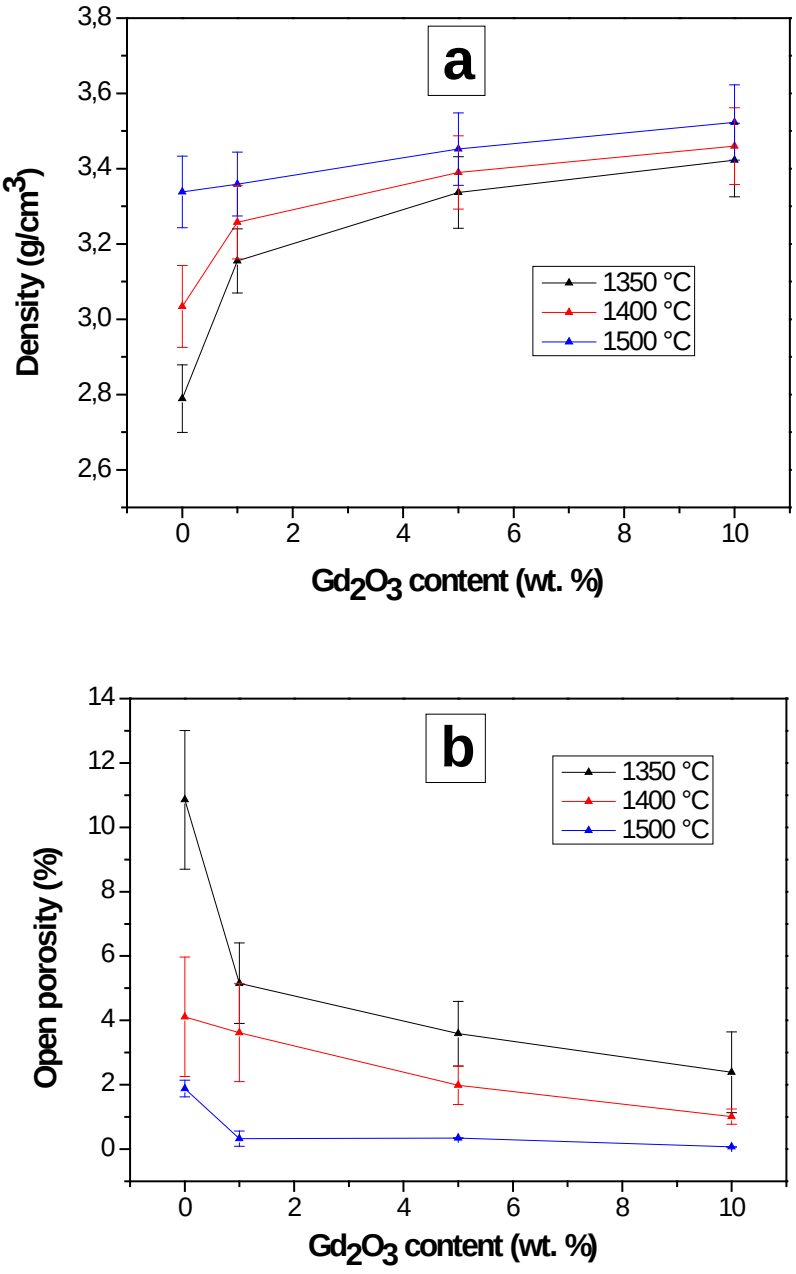

Fig. 5. Sintering parameters of the sintered mixtures at different heating programs (a) density; (b) porosity.

3.4 Microstructure developed (SEM)

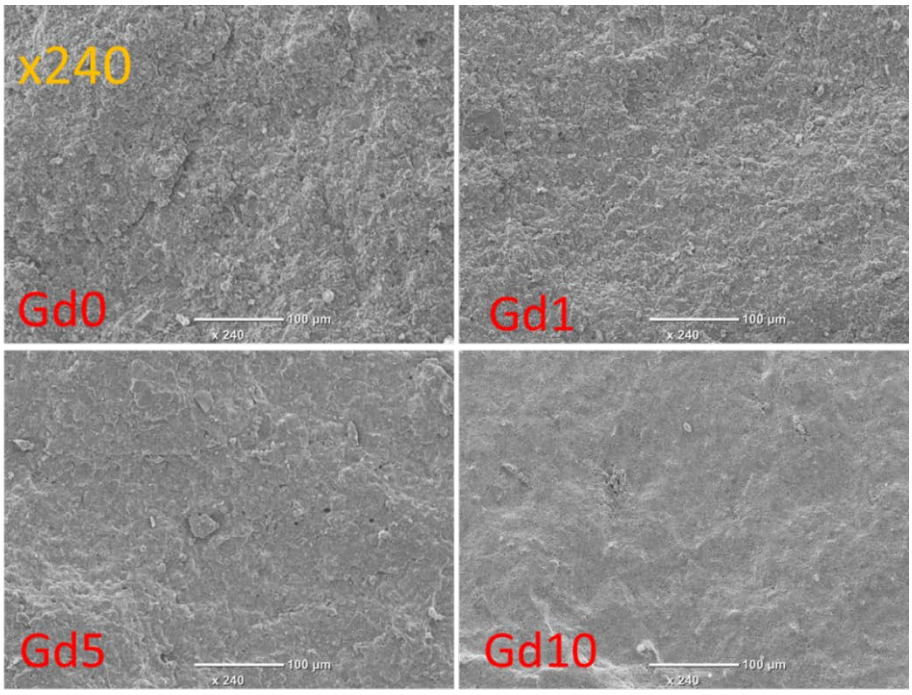

Fig. 6. Developed microstructure (x240) of the studied samples.

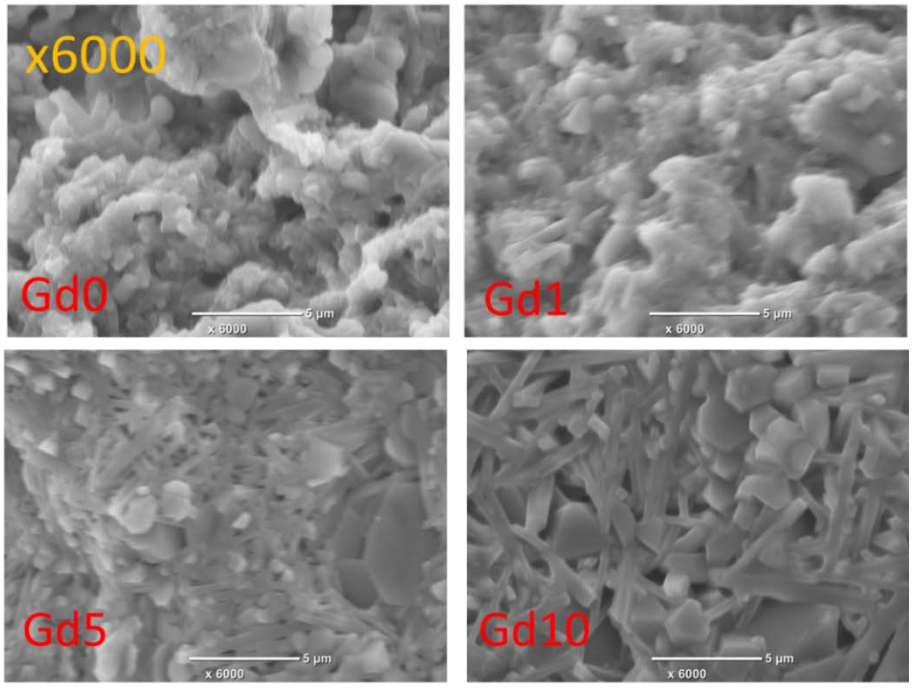

Fig. 7. Developed microstructure (x6000) of the studied samples.

The 1500 °C samples were chosen for the SEM analysis. These were fully dense in the immersion test. In the four cases, the observed microstructures are adequate for proppants manufacture. Homogeneous dense microstructures were achieved in the four studied samples

by the employed processing route, which corresponds to typical bauxitic proppants microstructures [2, 3, 38, 39]. No macro-pores were observed in the low enlargement SEM images (Fig. 6). The observed microstructures are easily illustrated in the x6000 SEM images. These correspond to the crystalline phase analysis (XRD-Rietveld analysis above) and the immersion test (Fig. 7). The sintered bauxitic sample (Gd0) presents a highly sintered alumina (Al_2O_3) grains microstructure. Rounded grains are observed, with no important amount of glassy phase present, results consistent with the XRD patterns as well.

On the other hand, the samples with rare earth content presented needle like grains imbibed in the sintered rounded grains microstructure (labeled in Figs. Gd1 and Gd5); only some needles are observed in Gd1 sample, in the Gd5 sample the needles proportion is high and comparable to the rounded alumina grains. These needle grains correspond to the observed crystalline phase belonging to the SiO_2-Gd_2O_3 and Al_2O_3-SiO_2-Gd_2O_3 systems [16] (see Section 3.2.). The needle morphology is similar to the mullite grains [28, 40, 44], under certain condition of growth stress strain induction in material during crystallization, crystals from in which the growth is rapid in one direction, developing filamentary crystals that are presumably free from gross imperfection [42]. This morphology might present a reinforcement mechanism in the materials [24, 35, 37], specially taking into account that these needles are generally monocrystalline, because they grow *in situ* during the thermal treatment [43]. Further analysis of this particular needle phase should be of interest, but falls out of the scope of this article.

The alumina grains are slightly larger than the grains observed in the sintered bauxite with no additives. This might be explained by secondary chemical processes that accompanied the needle growth.

Finally, in the Gd10 sample the needles are also observed and are the principal phase of the developed ceramic. The interlocking microstructure might present high mechanical performance [41, 42, 44]. As mentioned, the mechanical performance of the ceramics is a requirement for the proppant application [1]. However further studies should be carried out to reveal the actual behavior of these gadolinium aluminosilicate ceramics, which have been not reported before as structural ceramics.

3.5 Spatial distribution of Gd atoms

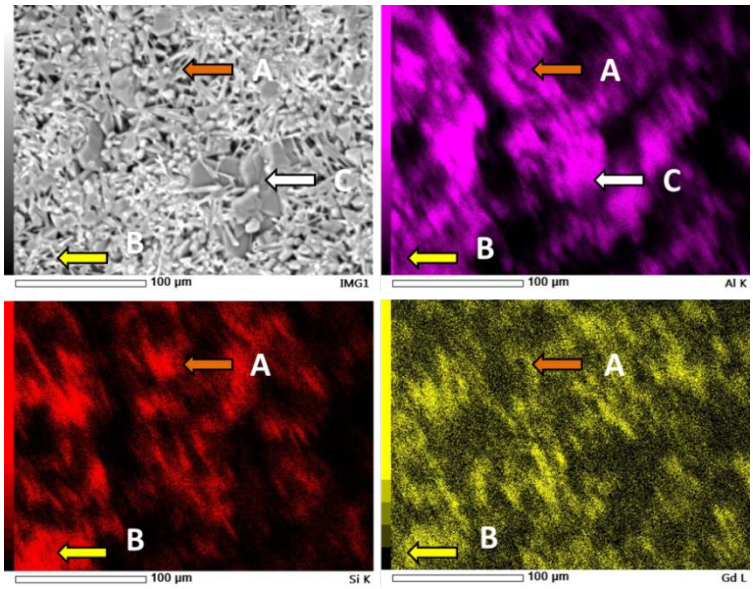

Fig. 8. SEM - EDS Mapping images of the Gd10 Material sintered at 1500 °C.

A simple EDS analysis was carried out to observe the gadolinium presence and visualize the spatial distribution. This is important in order to corroborate an isotropic and homogeneous distribution of this element when employed as a probe for neutron based detection technologies, as in the mentioned particular application; more so taking into account that proppants diameter is below one millimeter [1].

An element mapping of the Gd10 sample was carried out; illustrating the spatial distribution of the principal atoms. The original SEM image (grey) is accompanied by images corresponding to aluminum, silicon and gadolinium (violet, red and yellow correspondingly). Three points (A, B and C) were marked. A and B correspond to the needle zone and C to a sub angular-rounded grain. While the first ones correspond Al_2O_3-SiO_2-Gd_2O_3 system, the third one (C) corresponds to pure aluminum oxide. These results are in agreement with the XRD patterns (Section 3.2).

Finally, it could be stated that for practical purposes the degree of homogeneity of the spatial distribution of the high neutron capture atoms (Gd) is adequate for its use as a high neutron capture material.

3.6 Mechanical properties of the developed materials

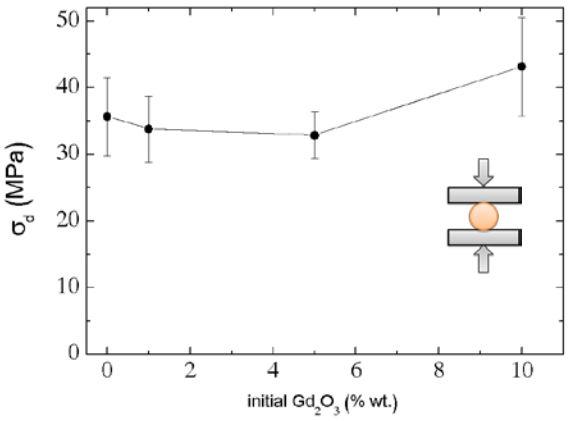

Fig. 9. Mechanical strain; diametral compression resistance of the studied samples as a function of the Gd_2O_3 content.

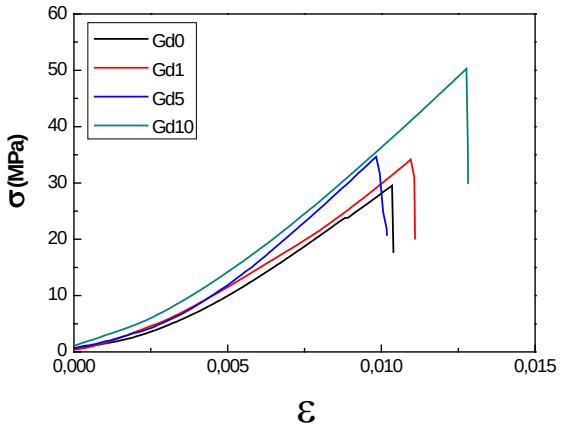

Fig. 10. Stress strain curves of the sintered bauxite Gd_2O_3 mixtures fired at 1500 °C (examples).

A simple mechanical behavior characterization was carried out for the fully densified materials sintered at 1500 °C. The results obtained might be to other geometries and processing routes [23].

The achieved mechanical strange encourages the structural application and the proppants design. Fig. 10 shows examples of the obtained stress strain curves. A fragile behavior was clearly observed in Gd0 and Gd10 the samples. The Gd1 and Gd5 specimens presents instability region originating from crack propagation, because of this a catastrophic rupture is not observed.

The effect of the Gd_2O_3 addition is observed: A slight decrease in the mechanical resistance is observed below 5 wt.% addition (approx. 10 wt.%). The Gd10 sample presented a higher mechanical resistance (20 % higher than the non-added bauxite-based ceramic). This is related to the needle microstructure (see Fig. 7) [44] and, as mentioned, could be an advantage in proppants usage [1,3].

3.7 Macroscopic neutron capture section (Σ) of the studied materials.

As expected, the incorporation of gadolinium increases considerably neutron capture section; and sustain the present application. The not added sample $\sum \approx 77$ c.u. and the 10 % wt sample is 1.5 x 10^5 c.u. The estimated values of $\sum$ [21] are almost linearly correlated (R^2=0.9975) with the amount of gadolinium oxide. The achieved values (see Fig. 11) ensures the detectability of proppants prepared with these content Gd_2O_3 content [16, 18].

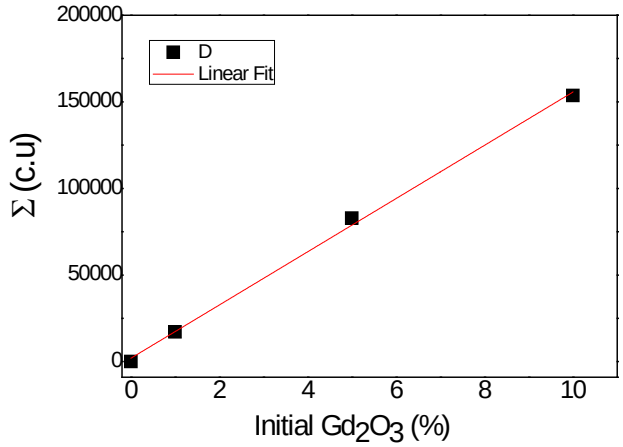

Fig.11. Macroscopic neutron capture section (Σ) of the studied materials as a function of the added Gd_2O_3 %wt.

4. Conclusion

The effect of a rare earth oxide (Gd_2O_3) addition in the thermal behavior of industrial bauxite and the technological properties of the resulting ceramics when fired at 1350-1500 °C were performed. A systematic formulation-sintering-properties correlation was carried out, characterizing also the non-added bauxite for comparison purposes. The incorporation of Gd_2O_3 is of technological interest for the design of smart traceable ceramic proppants used for unconventional gas and oil well stimulation. This high macroscopic neutron capture cross section proppants are used to obtain relevant information; such as the location and height of the hydraulically created fractures. The macroscopic neutron capture section ($\sum$) is almost linearly correlated with the oxide incorporation and was estimated up to 1.5 x 10^5 c.u for the

10%Gd; the estimated ∑ is considerably higher than any other reported ceramic proppants value, and represents an opportunity for designing ultra-high traceable proppants. Moreover, the 10 %wt. added sample resulted in better mechanical behavior.

The Gd_2O_3 addition did not affect the sintering starting temperature (1200 °C) but the sintering rate was increased. Dense, pore free ceramics, were obtained at lower temperatures. In all cases, the observed sintering differences could be optimized by later definitive heating programs. From this it could be stated that processing cost of the tagged proppants should only be increased by the raw materials cost.

The oxide role is different from the kaolinitic clay-based proppants, as no glassy phase was detected. Gd_2O_3 do not act as a fluxing agent when fired only with bauxite and the corresponding alumina phases, instead new gadolinium binary or ternary crystalline phases are formed. These phases present mullite needle like morphology; easily observed by SEM. This morphology resulted in a supplementary reinforcement mechanism. The mechanical behavior of the developed materials was not affected in the low Gd_2O_3 content samples (below 5 %) and increased the strength in a 20 the 10 % Gd_2O_3 added sample.

After this study, new high neutron capture proppants with good proppant performance can be designed with the developed materials.

Acknowledgments

This work has been partially supported by Nano-Petro FONARSEC Project 2012 (ANPCyT). Argentina; PICT-2016-0463 Argentina. MFH, JMM and RA acknowledge CONICET and Y-Tec for the fellowships respectively. The authors want to express their gratitude to Matias Gauna for the help in the SEM analysis.

5. References

1. F. Liang, M. Sayed, G. A. Al-Muntasheri, F. F. Chang, L. Li, A comprehensive review on proppant technologies, Petroleum. 2 (2016) 26-39.
2. A. Mocciaro, M. B. Lombardi, A. N. Scian, Effect of raw material milling on ceramic proppants properties, Appl. Clay Sci. 153 (2018) 90-94.
3. T. V. Vakalova, L. P. Devyashina, M. A. Burihina, A. S. Kisner, N. V. Pashenko, Alumosilicate ceramic proppants based on natural refractory raw materials, IOP Conf. Ser. Mater. Sci. Eng. 286 (2017) 012012.
4. T. V. Vakalova, V. M. Pogrebenkov, O. A. Chernousova, Structure-phase transitions upon firing of new ceramic feedstock, topaz-containing rocks, Steklo Keram. (2002) 24-27.
5. A. A. Reshetova, T. V. Vakalova, L. P. Govorova, E. A. Domukhovskaya, Influence of kaolin ignition temperature changes on the strength qualities of proppants, in: 2012 7th Int. Forum Strateg. Technol. IFOST, 2012: pp. 1-3.
6. A Green Alternative for Determination of Frac Height and Proppant Distribution - OnePetro, (n.d.). https://www.onepetro.org/conference-paper/SPE-138500-MS (accessed April 30, 2019).
7. J. Zhang, H. D. J. Smith, A Determination of the Capability of Using Gadolinium Tagged Proppant To Evaluate Propped Fracture Width, in: Society of Petrophysicists and Well-Log Analysts, 2017. https://www.onepetro.org/conference-paper/SPWLA-2017-AA (accessed January 17, 2020).
8. A. C. Ortiz, D. E. Hryb, J.R. Martínez, R. A. Varela, Hydraulic Fracture Height Estimation in an Unconventional Vertical Well in the Vaca Muerta Formation,

Neuquen Basin, Argentina, in: Society of Petroleum Engineers, 2016. https://doi.org/10.2118/179145-MS.
9. P. Saldungaray, R. J. Duenckel, T. T. Palisch, Reducing Hydraulic Fracturing HSE Footprint through the Application of a Non-Radioactive Method for Proppant Placement and Propped Fracture Height Assessment, in: Society of Petroleum Engineers, 2014. https://doi.org/10.2118/170333-MS.
10. M. F. Hernández, M. S. Conconi, M. Cipollone, M. S. Herrera, N. M. Rendtorff, Ceramic behavior of ball clay with gadolinium oxide (Gd_2O_3) addition, Appl. Clay Sci. 146 (2017) 380-387.
11. M. S. Herrera, M. F. Hernández, M. Cipollone, M. S. Conconi, N. M. Rendtorff, Thermal behavior of samarium oxide – Ball clay mixtures for high macroscopic neutron capture cross section ceramic materials, Appl. Clay Sci. 168 (2019) 125-135.
12. L. Andrini, M. R. Gauna, M. S. Conconi, G. Suarez, F. G. Requejo, E. F. Aglietti, N.M. Rendtorff, Extended and local structural description of a kaolinitic clay, its fired ceramics and intermediates: An XRD and XANES analysis, Appl. Clay Sci. 124-125 (2016) 39-45.
13. L. Andrini, R. Moreira Toja, M. R. Gauna, M. S. Conconi, F. G. Requejo, N. M. Rendtorff, Extended and local structural characterization of a natural and 800 °C fired Na-montmorillonite–Patagonian bentonite by XRD and Al/Si XANES, Appl. Clay Sci. 137 (2017) 233-240.
14. M. S. Conconi, M. R. Gauna, M. F. Serra, G. Suarez, E. F. Aglietti, N. M. Rendtorff, Quantitative firing transformations of a triaxial ceramic by X-ray diffraction methods, Ceramica. 60 (2014) 524-531.
15. M. F. Serra, M. S. Conconi, G. Suarez, E. F. Aglietti, N. M. Rendtorff, Volcanic ash as flux in clay based triaxial ceramic materials, effect of the firing temperature in phases and mechanical properties, Ceram. Int. 41 (2015) 6169-6177.
16. M. S. Herrera, A. Ortiz, D. Hryb, N. M. Rendtorff, Detectability of smart proppants traced with gadolinium and samarium in the Vaca Muerta formation, J. Pet. Sci. Eng. 179 (2019) 312-320.
17. R. J. Duenckel, T. T. Palisch, X. Han, P. Saldungaray, Environmental stewardship: Global applications of a nonradioactive method to identify proppant placement and propped-fracture height, SPE Prod. Oper. 29 (2014) 231-242.
18. J. Liu, F. Zhang, R. P. Gardner, G. Hou, Q. Zhang, H. Li, A method to evaluate hydraulic fracture using proppant detection, Appl. Radiat. Isot. 105 (2015) 139-143.
19. R. J. Duenckel, J. G. Leasure, T. Palisch, Improvements in Downhole Chemical Delivery: Development of Multifunctional Proppants, in: Society of Petroleum Engineers, 2014. https://doi.org/10.2118/168605-MS.
20. J. M. de Oliveira Neto, A. Yakovlev, The Use of Pre & Post Fracture Stimulation Logs To Better Integrate Static Petrophysical Analysis With Dynamic Data From Production Logs, in: Society of Petrophysicists and Well-Log Analysts, 2018. https://www.onepetro.org/conference-paper/SPWLA-2018-EEEE (accessed January 17, 2020).
21. D. V. Ellis, C. R. Case, J. M. Chiaramonte, Porosity from neutron logs I: Measurement, Petrophysics. 44 (2003) 383-395.
22. C. I. Torres, N. M. Rendtorff, M. Cipollone, E.F. Aglietti, G. Suárez, C.I. Torres, N.M. Rendtorff, M. Cipollone, E. F. Aglietti, G. Suárez, Comparative evaluation of properties of a clay based ceramic shaped via four techniques, Cerâmica. 64 (2018) 176-182.
23. W. M. Carty, U. Senapati, Porcelain-Raw Materials, Processing, Phase Evolution, and Mechanical Behavior, J. Am. Ceram. Soc. 81 (1998) 3-20.

24. N. M. Rendtorff, S. Gómez, M. R. Gauna, M. S. Conconi, G. Suarez, E. F. Aglietti, Dense mullite-zirconia-zirconium titanate ceramic composites by reaction sintering, Ceram. Int. 42 (2016) 1563-1572.
25. M. R. Gauna, M.S. Conconi, G. Suarez, E. Aglietti, N. M. Rendtorff, Dense zircon ($ZrSiO_4$) ceramics by a simple milling-sintering route, Sci. Sinter. 50 (2018) 15-28.
26. M. F. Hernández, G. Suárez, M. Cipollone, E. F. Aglietti, N. M. Rendtorff, Mechanical behavior and microstructure of porous needle: Aluminum borate ($Al_{18}B_4O_{33}$) and Al_2O_3-$Al_{18}B_4O_{33}$ composites, Ceram. Int. 43 (2017) 11759-11765.
27. M. L. Sandoval, M. H. Talou, A. G. Tomba Martinez, M. A. Camerucci, Mechanical testing of cordierite porous ceramics using high temperature diametral compression, J. Mater. Sci. 45 (2010) 5109-5117.
28. M. Laskou, G. Margomenou-Leonidopoulou, V. Balek, Thermal characterization of bauxite samples, J. Therm. Anal. Calorim. 84 (2006) 141-146.
29. K. Okada, N. ŌTsuka, J. Ossaka, Characterization of Spinel Phase Formed in the Kaolin Mullite Thermal Sequence, J. Am. Ceram. Soc. 69 (1986) C251-C253.
30. A. Terzić, V. V. Mitić, L. Kocić, Z. Radojević, S. Pašalić, Mechanical properties and microstructure fractal analysis of refractory bauxite concrete, Sci. Sinter. 47 (2015) 331-346.
31. Y. Li, H. Zhao, Effect of reduced al2o3 mole ratio on fabrication of cordierite ceramic by solid-state sintering method, Sci. Sinter. 51 (2019) 1-10.
32. M. F. Hernández, P. V. López, A. Violini, G. Suárez, M. S. Conconi, N. M. Rendtorff, Dense alumina-mullite composite ceramics from alumina and spodumene-albite feldspar binary mixtures: Processing and properties, Sci. Sinter. 51 (2019) 445-458.
33. C. Zanelli, M. Raimondo, G. Guarini, M. Dondi, The vitreous phase of porcelain stoneware: Composition, evolution during sintering and physical properties, J. Non-Cryst. Solids. 357 (2011) 3251-3260.
34. Phase evolution during reactive sintering by viscous flow: Disclosing the inner workings in porcelain stoneware firing–Science Direct, (n.d.). https://www.sciencedirect.com/science/article/pii/S095522191930874X (accessed January 16, 2020).
35. B. Ngayakamo, S. Eugene Park, Evaluation of kalalani vermiculite for production of high strength porcelain insulators, Sci. Sinter. 51 (2019) 1-10.
36. N. Tamari, I. Kondoh, T. Tanaka, H. Katsuki, Mechanical properties of alumina-mullite whisker composites, Nippon Seramikkusu Kyokai Gakujutsu Ronbunshi Journal Ceram. Soc. Jpn. 101 (1993) 721-724.
37. J. T. Kloprogge, H. D. Ruan, R. L. Frost, Thermal decomposition of bauxite minerals: Infrared emission spectroscopy of gibbsite, boehmite and diaspore, J. Mater. Sci. 37 (2002) 1121-1129.
38. M. Romero, J.M. Pérez, Relation between the microstructure and technological properties of porcelain stoneware. A review, Mater. Constr. 65 (2015) 065.
39. Toughening effect of mullite whisker within low-density ceramic proppants - Jianying Hao, Baolin Mu, Yunfeng Gao, Pinbo Bai, Yuming Tian, Guomin Li, 2019, (n.d.). https://journals.sagepub.com/doi/10.1177/2633366X19890625 (accessed January 16, 2020).
40. J. Hao, H. Hao, Y. Gao, X. Li, M. Qin, K. Wang, Effect of Sintering Temperature on Property of Low-Density Ceramic Proppant Adding Coal Gangue, Mater. Sci. 26 (2019) 94-98.
41. H. Schneider, J. Schreuer, B. Hildmann, Structure and properties of mullite—A review, J. Eur. Ceram. Soc. 28 (2008) 329-344.

42. P. F. Becher, T. N. Tiegs, J. C. Ogle, W. H. Warwick, Toughening of Ceramics by Whisker Reinforcement, in: R. C. Bradt, A. G. Evans, D. P. H. Hasselman, F. F. Lange (Eds.), Fract. Mech. Ceram., Springer US, Boston, MA, 1986: pp. 61-73.
43. K. Suganuma, T. Fujita, G. Sasaki, N. Suzuki, Evaluation of strength and heat-resistance for aluminum-borate whisker reinforced AC8A aluminum alloy composite, J. Jpn. Inst. Light Met. 41 (1991) 270-275.

Сажетак: *Предмет испитивања у овом раду је ефекат допирања боксита са до 10 мас.% гадолинијум оксида (Gd_2O_3) и термичко понашање добијеног материјала.Уграђивање (Gd_2O_3) је од интереса за технолошку примену у прављењу паметних керамичких материјала у индустрији нафте и гаса. Ови материјали имају велики макроскопски пречник за апсорпцију неутрона и користе се за добијање битних информација, као што су локација и висина хидрауличких фрактура коришћењем неутронских метода детекције.Овај рад садржи анализе понашања током термичког третмана и синтеровања до 1500 °C материјала са до 10 мас.% Gd_2O_3. Текстуре и морфологија добијених материјала су такође испитане, а обављена је и једноставна механичка карактеризација. Добијени су материјали максималне густине и без пора, са алумином и малитом као главним кристалним фазама. Секундарне и терцијарне алумино-силикатне фазе са гадолинијумом су такође нађене после загревања. Ове фазе имају игличасту морфологију која може да доведе до механизма ојачавања. Ниједна битна стакласта фаза није нађена; иако је синтеровање побољшано додатком гадолинијума, Gd_2O_3 поспешује синтеровање а не само проток масе. Материјал остаје механички ломљив и са додатком ретке земље. Механичка отпорност се повећала око 20 % за материјал допиран са 10 % Gd_2O_3. Додатак оксида са губитком масе због дехидроксилације оксида производи материјал са макроскопским пречником за апсорпцију неутрона од 1.5 x 105 (с.и.). Добијени резултати омогућавају развој стратегије дизајна материјала са великим макроскопским пречником за апсорпцију неутрона.*

Кључне речи*: боксит, ретке земље, гадолинијум оксид, паметни керамички материјали; термички пречником за апсорпцију неутрона.*